Available online at www.sciencedirect.com

ScienceDirect

Advances in Space Research 68 (2021) 275–291

ADVANCES IN SPACE RESEARCH (a COSPAR publication)

www.elsevier.com/locate/asr

Instrumental requirements for the study of Venus' cloud top using the UV imaging spectrometer VeSUV

Emmanuel Marcq [a,*], Franck Montmessin [a], Jérémie Lasue [b], Bruno Bézard [c], Kandis L. Jessup [d], Yeon Joo Lee [e], Colin F. Wilson [f], Benjamin Lustrement [a], Nicolas Rouanet [a], Gabriel Guignan [g]

[a] *LATMOS/IPSL, UVSQ, Université Paris-Saclay, Sorbonne Université, CNRS, Guyancourt, France*
[b] *IRAP, Université de Toulouse, CNRS, CNES, UPS, Toulouse, France*
[c] *LESIA, Observatoire de Paris, Université PSL, CNRS, Sorbonne Université, Université de Paris, 5 place Jules Janssen, Meudon, France*
[d] *Southwest Research Institute (SwRI), 1050 Walnut St., Suite 300, Boulder, CO 80302, USA*
[e] *Zentrum für Astronomie und Astrophysik, Technische Universität Berlin, Berlin, Germany*
[f] *AOPP, Clarendon Laboratory, Parks Road, Oxford OX1 3PU, UK*
[g] *LATMOS/IPSL, Sorbonne Université, UVSQ, CNRS, Paris, France*

Received 15 October 2020; received in revised form 4 February 2021; accepted 9 March 2021
Available online 24 March 2021

Abstract

Ultraviolet spectral imaging has been a powerful tool to investigate the cloud top of Venus, allowing for measurement of several minor gases (especially SO_2, SO, O_3), of cloud top aerosol's microphysical properties and of atmospheric dynamics through tracking of the unevenly distributed UV absorber. After a brief review of recent UV instruments that orbited around Venus, we present the results of a state-of-the-art radiative transfer model from Marcq et al. (2020) to derive the spectral resolution and Signal-to-Noise ratio (SNR) required to derive abundances of these gases, retrieve optical properties of the aerosols beyond our current knowledge. This leads us to propose a two-channel UV hyperspectral push-broom imager called VeSUV (standing for Venusian Spectroscopy in UV) whose technical characteristics will improve on existing measurements by a factor of at least 2, and which is well suited to the integration into the payload of future low Venus orbit platforms such as the proposed *EnVision* mission to ESA M5 call.

Keywords: Venus; Ultraviolet; Instrumentation; Atmosphere

1. Introduction

Although Venus displays very little contrast in the visible range, it is known since at least the late 1920s (Ross, 1928) that the spatial and spectral structure of the reflected sunlight at cloud top level is much richer in the near UV range, with a prominent absorption peaking near 365 nm (Heyden et al., 1959; Pollack et al., 1979; Pollack et al., 1980; Pérez-Hoyos et al., 2018). Permanent to semi-permanent spatial features include a characteristic Y-bow shape aligned with the zonal superrotation, as well as polar haze caps whose brightness varies on a multi-year timescale (Dollfus et al., 1960), as does the global UV albedo (Lee et al., 2019). This absorber is responsible for about half the total amount of absorbed sunlight in Venus' atmosphere, and thus plays a major role in the radiative balance and atmospheric dynamics (Haus et al., 2016).

The nature of this UV absorber is still debated, with candidate species as diverse as iron chloride (Zasova

* Corresponding author.
E-mail address: emmanuel.marcq@latmos.ipsl.fr (E. Marcq).

https://doi.org/10.1016/j.asr.2021.03.012
0273-1177/

et al., 1981; Krasnopolsky, 2017), disulphur dioxide (Frandsen et al., 2016; Frandsen et al., 2020) or various sulphur compounds (Hapke and Nelson, 1975; Toon et al., 1982), some even suggestingg a possible biological origin (Limaye et al., 2018). The chemical lifetime of this absorber near cloud top appears to be long relative to horizontal motions; this makes its absorption signature particularly suitable for short-term tracking of zonal and meridional winds at the cloud top (Khatuntsev et al., 2013; Hueso et al., 2015; Horinouchi et al., 2018). Readers interested in a more detailed review of UV cloud tracking are advised to refer to Sánchez-Lavega et al. (2017).

Another major insight provided by UV observations of Venus comes from spectroscopy, with the first detection of sulphur dioxide (SO_2) above the clouds by Barker (1979) using the space telescope International Ultraviolet Explorer (IUE). Subsequent observations of SO_2 absorption have been acquired over the decades from Venus orbiting missions, ground based observations and other space borne telescope platforms. After the first IUE observations, *Pioneer Venus* was the first to record strong temporal variability and a secular decrease in SO_2 abundance spanning two orders of magnitude in less than a decade (Esposito et al., 1979; Esposito et al., 1988), that could be a sign of a transient atmospheric destabilization through active volcanism (Esposito, 1984). After a relative neglect for a decade (1995 to 2005), similar near-decadal scale secular trends were inferred from the long-time base observations obtained by *Venus Express* (Marcq et al., 2011; Marcq et al., 2013; Marcq et al., 2020; Vandaele et al., 2017a; Vandaele et al., 2017b) while both ground-based (Encrenaz et al., 2012; Encrenaz et al., 2013; Encrenaz et al., 2016; Encrenaz et al., 2019; Encrenaz et al., 2020a; Jessup et al., 2015) and *Venus Express* observations confirmed that Venus' cloud top SO_2 abundance exhibit strong short-term as well as spatial variability. Other gaseous species detected at cloud top through their UV absorption are sulphur monoxide (SO) (Na et al., 1990; Na et al., 1994; Jessup et al., 2015) and even more recently ozone (O_3) (Marcq et al., 2019) – even though ozone was already known to exist at higher altitudes near 100 km thanks to UV stellar occultations (Montmessin et al., 2011).

Finally, the backscattered solar UV also provides clues to estimate the cloud top level aerosols' microphysical properties. The phase angle dependence at small phase angle, the so called optical glory phenomenon, is especially sensitive to a particle size and a variance of size distribution (García Muñoz et al., 2014; Markiewicz et al., 2014; Petrova et al., 2015a; Lee et al., 2017), especially when also including its degree of linear polarization (Kawabata et al., 1980; Knibbe et al., 1998; Braak et al., 2002). Their local time variations have been poorly understood, even though the photochemical aerosol formation process is directly linked to the SO_2 and SO gases that will be measured simultaneously.

Both ESA's *Venus Express* (2006–2014) (Titov et al., 2006) and JAXA's *Akatsuki* (2015-) (Nakamura et al., 2016) orbiters include UV sensitive instruments, whose description and main results are detailed in the next section Section 2. Section 3 deals with the expected accuracy of UV measurements with respect to SNR and spectral resolution, as well as required spatial resolution. Finally, Section 4 describes a UV instrument concept whose technical specifications allow for a significant improvement on the previous measurements according to our modeling.

2. Recent Scientific heritage

In this section, we summarize the most recent UV datasets available for Venus, in order to assess how we can improve on their results.

2.1. UV Spectroscopy

2.1.1. Low-resolution

SPICAV-UV was the UV channel of the SPICAV spectrometer suite (Bertaux et al., 2007) on board ESA's orbiter *Venus Express*. It was able to operate in stellar occultation mode, as well as in nadir or near-nadir viewing geometry. Its spectral resolution was ~ 1.5 nm over the 110–320 nm interval.

In the nadir mode, SPICAV explored Venus' dayside cloud top UV signature (Marcq et al., 2011; Marcq et al., 2013; Marcq et al., 2020). These studies recorded the cloud top sulphur dioxide SO_2 abundance thanks to its absorption bands centered near 215 and 283 nm, and a plausible range of sulphur monoxide SO thanks to its absorption band centered near 215 nm. Marcq et al. (2019) then discovered about 10 ppbv of ozone O_3 thanks to its so-called Hartley absorption band centered near 255 nm.

It could also measure the UV reflectance of the cloud top out of any absorption bands from atmospheric gases, thereby yielding constraints on the unknown UV absorber spatial and temporal variability – although its UV absorption is maximal near 365 nm, absorption is still noticeable at shorter wavelengths (Pérez-Hoyos et al., 2018; Marcq et al., 2019).

The moderate spectral resolution of SPICAV-UV only allowed the observation of absorption bands rather than resolving the individual absorption lines that make up these bands (Fig. 1). Therefore, it suffered from several degeneracies: between SO_2 and SO, so that the SO:SO_2 ratio had to be assumed (usually 10%, based on high resolution spectroscopic studies detailed in Section 2.1.2), but also between the cloud top altitude (measured using the strong CO_2 absorption at wavelengths shorter than 220 nm) and the spectral slope of the UV absorber (Marcq et al., 2020).

SPICAV-UV confirmed the very high variability of SO_2 above cloud top already evidenced by OUVS on board *Pioneer Venus* two decades earlier. Two different regimes of vertical transport were established by Marcq et al. (2013): one with a higher abundance in SO_2 and a decreasing trend with increasing latitude in both hemispheres, consistent

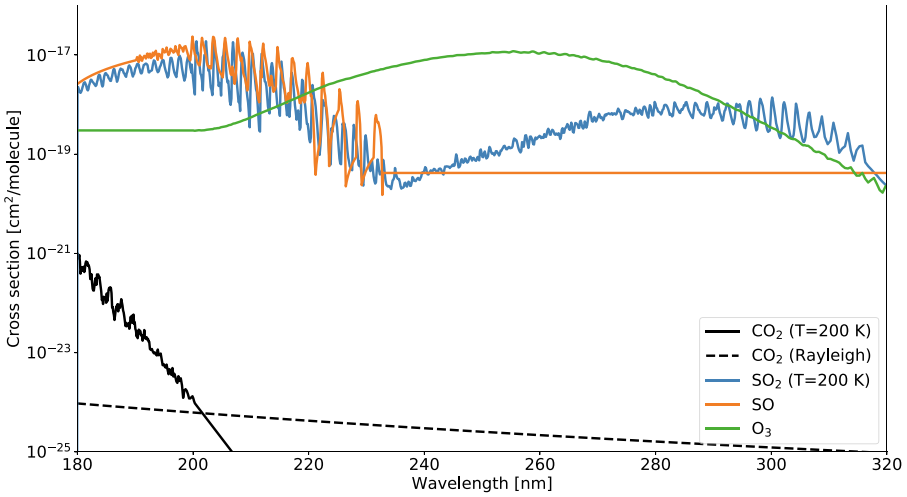

Fig. 1. Absorption cross-sections of gaseous minor species in the spectral range observed by SPICAV-UV. SO_2 cross-section is identical to Jessup et al. (2015), whereas SO cross-section from 190 to 230 nm is taken from Phillips (1981) and extrapolated beyond. O_3 cross-section comes from Sander et al. (2003) at wavelengths larger than 205 nm, and CO_2 absorption cross-section from Parkinson (2003) – Rayleigh scattering from CO_2 from Sneep and Ubachs (2005).

with an efficient supply of SO_2 from the lower atmosphere via vertical transport at low latitudes. And then, another with a much lower abundance in SO_2 and a suppression (or even a reversal) of the latitudinal gradient, suggesting during these periods the inefficient resupply of SO_2 via vertical transport. The SO_2-rich regime was more prevalent in the earlier part of the mission (2006 to 2010), whereas the SO_2-poor regime dominated the second half of the mission. These data also revealed a temporal anti-correlation between the UV absorber and SO_2 (Marcq et al., 2020), hinting at a possible conversion between both species which if proven true would support the hypothesis of a sulphur-bearing UV absorber.

2.1.2. High-resolution

Currently available UV spectroscopic observations with the highest spectral resolution (0.27 nm) were performed by the STIS imaging spectrometer on board the Hubble Space Telescope (HST). Despite the difficulty of pointing at a target (Venus) so close to the Sun, Jessup et al. (2015) could acquire spectra along six slits positions on the day side of Venus, on Dec. 28th 2010, Jan. 22nd 2011 and Jan. 27th 2011. These spectra had a spatial sampling of ~ 50 km and covered the 170–317 nm spectral range. Jessup et al. (2015, their Fig. 3) show a typical spectrum, that exhibits distinct absorption lines of both sulphur oxides SO and SO_2, thus enabling separate measurements with a typical retrieval accuracy of $\sim 20\%$ for both SO and SO_2 and within a factor of 2 for their ratio (Jessup et al., 2015, their Fig. 8).

From these observations, Jessup et al. (2015) were able to confirm the inversion of the latitudinal gradient of SO_2 within a month, supporting the theory that these distributions are directly related to variable periods of high and low SO_2 vertical mixing first reported by SPICAV-UV (Marcq et al., 2011; Marcq et al., 2013). SO and SO_2 were found to be highly correlated, with typical SO:SO_2 ratios ranging from 7 to 18%. The absolute UV cloud brightness derived from the Hubble observations was also used to support the assignment of the absolute 365 nm brightness evident in the VMC and *Akatsuki* images obtained at similar observational phase angles (Section 2.2). This work led to the identification of a multi-year decreasing trend in the cloud top albedo (Lee et al., 2019). This darkening trend was also evident in the SPICAV observations, in addition to the strong anti-correlation in the abundances of the unknown UV absorber and SO_2 gas at the cloud top (Marcq et al., 2020).

2.2. UV Imaging

In contrast to the aforementioned spectrometers, UV imagers emphasize wide field-of-views and spatial (angular) resolution at the expense of the wavelength coverage (usually a few discrete wavelengths through narrow band filters). The most recent ones have been VMC (Markiewicz et al., 2007) on board *Venus Express*, as well as UVI (Yamazaki et al., 2018) on board JAXA's orbiter *Akatsuki*. We will also discuss in this section the VIRTIS-M data (Drossart et al., 2007) aboard *Venus Express*. This instrument was an imaging spectrometer of relatively low spectral resolution, ans most of its science exploitation in its UV–visible range was performed using it as an imager at several wavelengths, which is why we list it in this section rather than the previous one.

Both instruments VMC and UVI have comparable specifications: UVI observations were performed at 283 and 365 nm (focusing on SO_2 absorption and the unknown UV absorber respectively), whereas VMC's only UV filter is also centered on 365 nm where spatial UV contrasts are maximal. UVI has a field-of view of $12^\circ \times 12^\circ$ (VMC: $17.5^\circ \times 17.5^\circ$), and its angular sampling is 0.2 mrad

(VMC: 0.7 mrad). Depending on the altitude of their respective orbital platforms, this translates into spatial sampling at cloud level ranging from 0.2 to 76 km according to Yamazaki et al. (2018) (VMC: from 0.2 to 45 km).

This spatial resolution enabled detection of UV contrasts ranging from planetary scale (like the aforementioned Y-bow shape) to mesoscale: sub-solar mottled convection patterns (Titov et al., 2012, their Fig. 7), middle latitude streaks (Titov et al., 2008) or gravity waves (Piccialli et al., 2014) whose spatial wavelengths range from 3 to 20 km. They could also track these UV contrasts as proxy for horizontal wind speeds (Khatuntsev et al., 2013; Horinouchi et al., 2018) and monitor the long term evolution of the 365 nm albedo (Lee et al., 2015). The vertical distribution of the UV absorber was also suggested to vary over the 5 years of *Venus Express* (Lee et al., 2015). The global view of UVI helped to find a clear correlation between the UV absorbers (SO_2 and the unknown absorber) and the cloud top altitudes inferred from the CO_2 absorption band at 2.02 μm (Lee et al., 2020). Their finding implies that the UV absorbers' abundances and the cloud top altitude are associated with a common atmospheric dynamics, such as the global scale planetary waves.

Study of the UV phase function of Venus has also been performed by both VMC (Markiewicz et al., 2014; Petrova et al., 2015a) and UVI (Lee et al., 2017). Thanks to the glory backscattering feature peaking near a phase angle of 10°, they could constrain the effective radius of the so-called "mode 2 particles" (which constitute the bulk of the upper and middle opacity in the visible–UV range) between 1 and 1.4 μm with a comparatively small variance in size distribution, with evidence for a decrease of their effective radius with increasing latitude on the morning side. Interestingly, the retrieved refractive index of these particles was found to exceed the value for pure H_2SO_4 whereas IR observational constraints rather point to a H_2SO_4:H_2O ratio ranging between 75% and 90% (Barstow et al., 2012; Arney et al., 2014). This suggests a contamination of these droplets with contaminants that may also be candidates for the UV absorber, e.g. sulphur and/or chlorine based compounds (Petrova et al., 2015a; Petrova et al., 2015b). Finally, taking advantage of the wide array of observational geometries allowed by the large FoV of VMC, Molaverdikhani et al. (2012) were able to constrain the vertical distribution of the UV absorber (well mixed above 63 km or restricted to a thin layer near 71 km) and well as its latitudinal variations (365 nm optical depth halved near both poles compared to the equator).

On the other hand, VIRTIS-M-vis was an imaging spectrometer covering the 270–1100 nm range with a spectral sampling of about 2 nm with a 0.25×64 mrad^2 ($\approx 0.015^\circ \times 3.4^\circ$) instantaneous field of view. Full spectral cubes could be obtained through scanning the second spatial dimension using the secondary telescope mirror. Its spectroscopic capabilites were somewhat hampered by straylight and calibration issues, therefore most of its scientific results came from UV imagery instead. In particular, upper cloud tracking in the 360–400 nm was performed by Hueso et al. (2015), constraining the global circulation and wind shear in relation with dynamics at other levels (Sánchez-Lavega et al., 2016; Hueso et al., 2012), and hinting at an intense atmospheric wave activity. These waves were studied previously by Peralta et al. (2008) who observed wavepackets over high southern latitudes extending for several hundreds of kilometers, a typical wavelength in the 90–320 km range, with a zonal velocity of a few tens of m/s relatively to the local zonal wind speed. The typical spatial resolution of the VIRTIS-M data used for atmospheric dynamics studies was in the range 16–50 km. In contrast with the shorter wavelength systems observed by Piccialli et al. (2014), these scarcely occuring wave packets exhibited no correlation with high topographic features.

3. Scientific requirements

Based on the aforementioned review of the most recent UV observations of Venus, we can formulate the following scientific objectives for our proposed UV investigation as included in the payload of a low Venusian orbiter similar to the ESA M5 candidate mission *EnVision* described here below.

3.1. The proposed EnVision mission

3.1.1. EnVision science goals

The *EnVision* mission (Ghail et al., 2017) lies at the heart of the ESA *Cosmic Vision* programme whose objectives are to identify the conditions for planet formation and the emergence of life, and to understand how the Solar System works. In this context, *EnVision* is dedicated to the study of the Venus planet. The key questions for this mission to address are linked to:

1. *Activity* How geologically active is Venus?
2. *History* How have the surface and interior of Venus evolved?
3. *Climate* How are Venus' atmosphere and climate shaped by geological processes?

The payload of *EnVision* shall include a synthetic aperture radar, a radio science experiment, a subsurface radar sounder and finally a spectrometer suite named *VenSpec* (Helbert et al., 2019) including three instruments: the thermal IR imager *VenSpec-M*, the high-resolution IR spectrometer *VenSpec-H*, and finally the *VeSUV* instrument as its UV channel *VenSpec-U*.

3.1.2. VenSpec-U science goals

The VenSpec-U project is part of the *EnVision* mission as a core element whose main scientific objectives are to:

– *Search for atmospheric effects of geological activity*, in order to determine how much outgassing is occurring (if any), and how the atmospheric chemistry is coupled with surface and subsurface geochemistry and weathering cycles.
– *Study how mesospheric gas variations are linked to possible volcanic activity*, in order to identify the causes of variability in the mesospheric sulphur dioxide.
– *Study how cloud and particulate variability is linked to possible volcanic activity*, in order to detect plumes of volcanic ash or sulphate clouds that volcanism would cause, and to understand any link between the Venus sulphuric acid cloud and the possible volcanic activity.

The VenSpec-U/VeSUV project is consequently primarily dedicated to the monitoring of the distribution and spatial and temporal variations of sulphur-bearing gases (SO, SO_2) and unknown particulate absorber at the cloud tops, through spectral analysis of backscattered sunlight on the dayside of Venus. When combined with the two other IR sensitive channels included in the VenSpec suite, detailed studies of the chemistry and transport supporting Venus sulphur species distributions between the surface and the cloud top may be completed: for example combining -U channel SO_x measurements with high resolution IR spectra from the -H channel yielding H_2O and OCS measurements both below and above the clouds will provide critical data needed to study Venus' aerosol formation process. Considering the focus on gaseous measurements, no additional polarimetric capability is expected at this stage.

Finally, it should be noted that nadir (or nadir-like) spectroscopy using backscattered sunlight is only sensitive to column densities above an effective backscattering altitude – about 70 km in the UV range (Marcq et al., 2019), which defines the effective cloud top altitude. Conversion into local mixing ratios relies on external assumptions for the vertical profiles of the considered species and scattering species (whether particulate or gaseous).

SO_2 SPICAV-UV typical relative accuracy was in the 20% to 50% range, which was enough to characterize the spatial and temporal variability of SO_2. However, there were some (< 10% of the total) observations where SO_2 fell below its detection threshold (about a few ppb at 70 km). Taking into account the improvements in UV sensor technology, and in order to better characterize the low SO_2 regime, we aim for a 2-fold improvement in our SO_2 relative accuracy compared to SPICAV-UV (10% relative uncertainty).

SO A better understanding of the sulphur chemistry at cloud top level requires simultaneous measurements of SO_2 and SO with a comparable accuracy. Existing HST-STIS data only constrain their ratio within a factor of 2, we aim here for a relative accuracy on the SO:SO_2 of 20% or better. Another indirect motivation for this value comes from minimizing the bias on SO_2 measurements caused by assuming a wrong value of the SO:SO_2 ratio (see Section 3.3.2).

UV absorber Since this absorber acts as a tracer for the convective activity responsible for the SO_2 supply at cloud top, monitoring the spatial and spectroscopic variations in UV range caused by this absorber is fully included in our sulphur chemistry investigations.

Cloud particles Finally, the interplay between gaseous and condensed phases within the clouds is also poorly understood. Any insight about the UV scattering particles that can be obtained from UV observations would help in understanding the highly coupled microphysics, homogeneous and heterogeneous chemistry processes that take place at cloud top level.

Also, all the above mentioned measurements should be as representative as possible in order to build a full climatology of the observable parameters. Therefore, a global coverage in excess of 60% of the whole day side (with respect to latitude, longitude and local solar time) is needed, with any gaps as small as possible (< 10% in any dimension) and if possible minimizing any spurious correlation.

3.1.3. Observation strategy

Radar observations require a spacecraft altitude as low as possible, and ideally a circular orbit. Spatial coverage, mass and budget considerations resulted in several trade-offs, resulting in a planned low eccentricity polar orbit whose altitude varies between about 150 and 525 km (period: 94 min), with a variable pericenter latitude (low to middle latitudes) during the planned duration of the mission. This working orbit requires an initial two year long aerobraking phase during which no scientific observations are possible (mainly due to heat dissipation). Therefore, no instrument can get a synoptic instantaneous hemispheric coverage on board *EnVision*.

Instead, the most cost-effective solution to enable both imaging and spectroscopic capabilities in this orbital configuration is the so-called "pushbroom" observation mode, with the nadir observed swath slowly precessing with each orbit relative to the Venusian surface. This will also allow for successive observations relative the same ground spot, which will help in addressing the topic of surface-atmosphere interactions (see Section 3.2.3).

Data link rate is also a primary concern for *EnVision*, so that one instrument cannot operate continuously. In the current version of the operation scenario, VenSpec-U is allowed to operate for four consecutive dayside half-orbits every 16 orbits (totalling 24 Earth hours). This enables the above mentioned short-term overlapping, and results in a > 90% global planetary coverage (relative to

the surface) at the end of the nominal mission (6 Venusian sidereal days, or "cycles").

3.2. Spatial requirements

The spatial resolution requirements would be driven mainly by our need to understand the vertical transport as well as interactions of the sulphured gaseous species with clouds – more specifically, resolving convection and wave-cloud interactions. On the other hand, long term, climatological mapping of sulphured gases would only need large scale measurements over a longer time period.

3.2.1. Support from previous observations

In order to assess more quantitatively the horizontal scales visible in the UV range, we have performed a high pass filtering (at a 1σ 10-km length scale) for some publicly available 365 nm images from the UVI instrument on board *Akatsuki* with the finest spatial resolution available, less than 3 km/pixel (Fig. 2). Significant convective and wave activity can be seen for typical length scales of a few kilometers.

Interestingly, this 1-10 km length scale arises in two different, unrelated phenomena. First of all, this kilometric length scale is consistent with the smaller features observed by VMC on board *Venus Express* and already mentioned in Section 2.2, like mottled convective features close to the subsolar point (Titov et al., 2008). Aside from convective activity, the other kind of dynamical targets we may investigate at this wavescale would be orography-induced gravity wave activity, e.g. near *Maxwell Montes*. Piccialli et al. (2014) have measured wavelengths ranging from 3 to 20 km, in the same order of magnitude as the above described convective features. Similar correlations with topography were also found for intermediate wavelength systems (Peralta et al., 2017) and planetary-scale bow wave (Fukuhara et al., 2017; Kitahara et al., 2019). However, the long wavesystems found by Peralta et al. (2008) at various cloud altitudes did not correlate with any surface features.

3.2.2. Support from mesoscale modeling

Another clue showing the scientific importance of the $\sim$ 10 km horizontal scale length comes from the LMD-IPSL mesoscale models of the atmosphere of Venus (Lefèvre et al., 2017; Lefèvre et al., 2018). This model includes visible and IR radiative forcing by gases and aerosols, and can simulate (Fig. 3) the convective activity observed at cloud top near the subsolar point (Titov et al., 2008). In these simulations, the spatial extent of the convection cells (in which the UV absorber acts as a tracer) is confirmed to be on the order of $\sim$ 10 km. Furthermore, these mesoscales simualtions predict that cloud top convection is restricted to lower latitudes and caused by static instabilty caused by localised UV solar heating, leading to shallow convection as suggested by Imamura et al. (2014).

Also, the similarity between the simulated vertical wind vector field and the observed convection cells implies that the observed small scale mottled contrasts would be connected with wind vectors. High spatial resolution observations could quantify this possible correlation between vertical motions and UV brightness, and would explain how the UV absorber abundances or fresh bright cloud area are evolving over upwelling or downwelling areas.

Other mesoscale simulations were performed by Imamura et al. (2014) using the "Cloud Resolving Storm Simulator". They also concluded that the horizontal scale of convection cells is typically in the 10–15 km interval.

3.2.3. Spatial Field-of-view (FoV)

The extent of the spatial transverse FoV is mainly dictated by the need to observe the spatial structure of the backscattered light over a swath at least several times larger than the above mentioned 10 km spatial scale. For an instrument located in low Venusian orbit (220 km), this translates into an angular transverse FoV of at least 20°. This brings two additional advantages:

– if the instrument is carried on a polar orbit, it allows for several successive (low Venusian orbit has a $\sim$ 80 min period) nadir observations over the same ground spot,

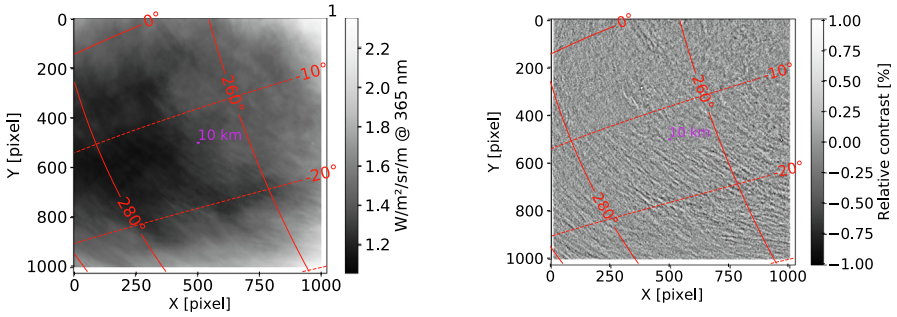

Fig. 2. *Left:* Calibrated UVI image of Venus acquired from *Akatsuki* spacecraft on 2016–09-04. Red lines show the latitude/longitude grid. 1 pixel equals 3 km at cloud top level at the center of this image. *Right:* High-pass filter applied to the left image, computed as local relative departure between the calibrated image shown left and its 10 km gaussian smoothed version. (For interpretation of the references to colour in this figure legend, the reader is referred to the web version of this article.)

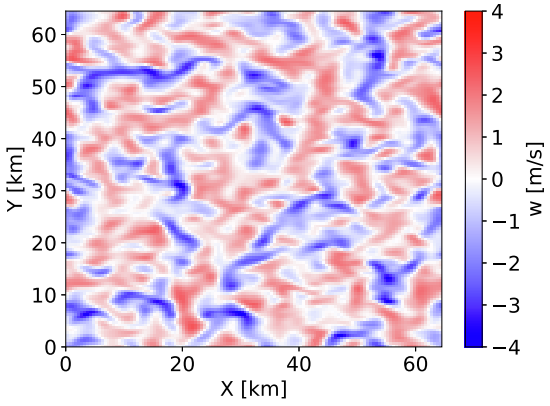

Fig. 3. Horizontal cut of the instantaneous vertical wind at an altitude of 70 km at the subsolar point from the mesoscale model of Lefèvre et al. (2018).

since the orbit will only slowly precess relative to the Venusian surface in a slow rotation. Also, since the zonal superrotation will renew the atmospheric content at cloud top between two consecutive observations, any significant correlation between these consecutive observations could be traced back to the influence of the solid surface at the cloud top level. Kouyama et al. (2017,) and Kitahara et al. (2019) showed local time dependence of topographic waves in images recorded by *Akatsuki* in the thermal infrared of cloud top near 10 μm as well as near 283 nm. This makes the study of gravity waves and their local time dependence possible, further constraining dynamical modeling at both global level (Navarro et al., 2018) and mesoscale level (Lefèvre et al., 2020).

– A 20° wide FoV also allows for observations over a similar phase angle range, especially if some observations are performed with an emission angle different from 0°. This could better constrain the phase function of the upper clouds and hazes for several wavelengths bins over the spectral range of VeSUV. More specifically, in strict nadir viewing and near the subsolar point, the already mentioned glory feature, occurring only for phase angles near $\sim 10^{\circ}$, could be observed and help in constraining the cloud particle size distribution and refractive index/composition (Markiewicz et al., 2018; Markiewicz et al., 2014; Rossi et al., 2015).

3.3. Signal-to-Noise & spectral requirements

3.3.1. Radiative transfer methods

The forward model of Venus' UV spectral reflectance first developed by Marcq et al. (2011), updated for Marcq et al. (2013) and Jessup et al. (2015) and more recently for Marcq et al. (2019, 2020) makes use of line resolving, high resolution gaseous absorption cross-sections. This model can be run using vast array of wavelength ranges and spectral resolutions.

In order to better constrain the accuracy of SO_2 and SO measurements derived from spectroscopic observations of Venus' cloud top, we adopted the following scheme:

1. Synthetic computation of a typical dayside reflectance spectrum of Venus observed at nadir ($SO:SO_2$ ratio set at 0.1, solar zenith angle of 30°, emission angle of 0°, SO_2 abundance of 10 ppbv set at 70 km, cloud top set at 73 km, imaginary index of so-called "mode 2" particles is set at $3 \cdot 10^{-2}$ at 250 nm;
2. Adding of a synthetic noise whose spectral variations follow the noise expected from the reflected spectrum. This noise is then scaled to a given value of Signal-to-Noise Ratio (SNR) set at a reference wavelength of 240 nm;
3. Retrievals using a Levenberg–Marquardt algorithm (Newville et al., 2020) based on the synthetic noised spectrum described above:
   (a) on the 190 to 320 nm interval, similar to SPICAV-UV spectral range and sampled at twice the assumed spectral resolution, $SO:SO_2$ ratio set at 0.1, cloud top altitude, imaginary index and SO_2 abundance left as free parameters. Such a setup is identical to the fitting strategy used by Marcq et al. (2020);
   (b) on the 200 to 240 nm interval, similar to HST/STIS spectral range and sampled at twice the assumed spectral resolution, cloud top altitude set at 73 km, $SO:SO_2$ ratio, imaginary index and SO_2 abundance left as free parameters.

3.3.2. Results

After having run the above described forward model for several values of scaled SNR and spectral resolution, we show in Fig. 4 the relative accuracy – defined as the standard error yielded by the Levenberg–Marquardt fitting algorithm divided by the prescribed parameter value – for retrieved SO_2 (assuming a fixed $SO:SO_2$ ratio) on the 190–320 nm range, and for $SO:SO_2$ ratio on the 200–240 nm range (assuming a fixed cloud top altitude). Unsurprisingly, larger SNR values lead to a much improved accuracy, as well as improved spectral resolution/sampling.

However, $SO:SO_2$ ratio retrieval on the narrow band 200–240 nm – where SO exhibits a well characterized absorption cross-section (Phillips, 1981) – is relatively more sensitive to spectral resolution vs. SNR compared to SO_2 retrievals – the logarithmic slope of iso-accuracy lines on Fig. 4 is 40% steeper for $SO:SO_2$ ratio compared to SO_2 abundance. This is due to the fact that distinguishing between SO and SO_2 absorption requires that the individual absorption lines (and not only the absorption bands) are resolved on the spectrum, which is the case only for a spectral resolution smaller than 1 nm (Fig. 5).

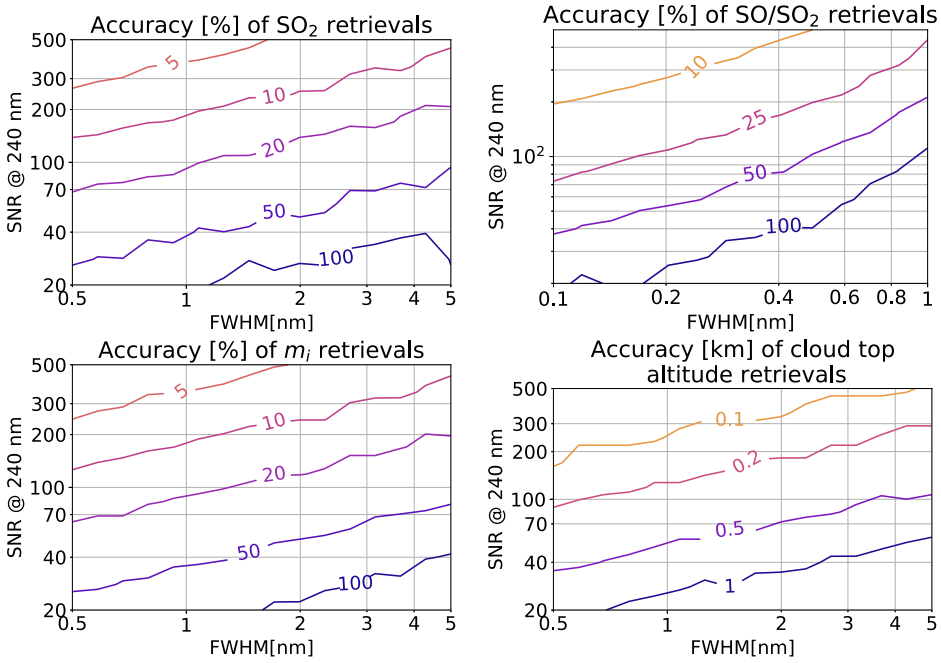

Fig. 4. *Upper left:* relative accuracy of SO_2 retrievals with respect to SNR at 250 nm and spectral resolution full width half maximum (FWHM). *Upper right:* relative accuracy of SO_2 retrievals with respect to 250 nm SNR and spectral FWHM. *Lower left:* relative accuracy of imaginary index retrievals with respect to 250 nm SNR and spectral FWHM. *Lower right:* Accuracy (in km) of cloud top altitude retrievals with respect to 250 nm SNR and spectral FWHM.

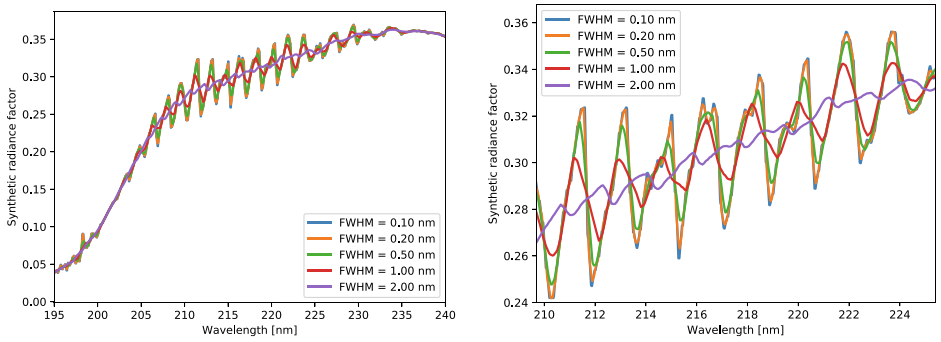

Fig. 5. Simulated radiance factors in the nominal case for various spectral full width half maxima (FWHM) using our forward model.

Also, it is interesting to compare these modeled relative accuracies with those derived from similar observations. The latest SPICAV-UV measurements (Marcq et al., 2020) typically yielded SO_2 measurements with a relative uncertainty (error interval width divided by retrieved value) of 25 to 50%, whereas HST/STIS line resolving observations by Jessup et al. (2015) had a typical relative uncertainty of about 50% for their retrieved SO:SO_2 ratio.

Keeping these values in mind, we used our forward model to investigate the bias on SO_2 retrievals if the assumed SO:SO_2 ratio differs from its actual value. We found that a 100% increase in the assumed vs. actual SO:SO_2 ratio leads to a 25% overestimation of the retrieved SO_2 abundance compared to its prescribed value. Therefore, in order to maintain a precision of our SO_2 retrieved value well within our 10% error margin goal, we must measure simultaneously the SO:SO_2 ratio with an accuracy much better than 40%. Our target value of a 25% relative precision for the SO:SO_2 ratio measurements fulfills this constraint.

3.3.3. Spectral range

Although the longer wavelengths within the SPICAV-UV spectral range already pointed to an increasing absorption (Marcq et al., 2019; Marcq et al., 2020), it could not acquire reflectance data beyond 320 nm. In principle, the visible channel (0.25-1 μm) of the VIRTIS-M spectral imager (Drossart et al., 2007) would have bridged the gap to the absorption peak of the unknown UV absorber located near 365 nm, but cross-calibration between VIRTIS and SPICAV appeared difficult to reach in the 300–400 nm range (Vlasov et al., 2019). Opportunistic spectral measurements over the whole 0.2-1.4 μm range have been acquired by Pérez-Hoyos et al. (2018) using the MASCS spectrome-

ter on board NASA's *Messenger* mission to Mercury. They evidenced smooth spectral variations of their retrieved imaginary index of cloud particles in the 300–600 nm interval and could rule out some possible compositions for the UV absorber based on these measurements, e.g. croconic acid (Hartley et al., 1989), S_4 (Hapke and Nelson, 1975), or nitrosylsulphuric acid (Watson et al., 1979).

In order to constrain the spectral properties of the "unknown UV absorber" the spectral range of VeSUV must therefore reach at least 365 nm. However, only a moderate spectral resolution is required considering that no narrow spectral features have ever been measured in this range, which would be consistent with a UV absorber embedded in a condensed phase.

3.4. Science traceability matrix

As a summary of this section, Table 1 shows a science traceability matrix for the VeSUV instrument, relating science objectives to instrumental specifications.

4. Instrumental concept

Here we present the so called VeSUV (standing for *Ve*nus *S*pectrography in *U*ltra*V*iolet) instrument concept, which fulfills the requirements detailed in Section 3. In the context of the candidate ESA M5 proposal *EnVision*, VeSUV is part of a spectrometer suite called VenSpec (Helbert et al., 2019), and therefore primarily known as VenSpec-U.

4.1. Instrument description

The VenSpec-U instrument is a dual channel UV spectral imager. The low spectral resolution "LR" channel ranges from 190 to 380 nm at a 2 nm spectral resolution and a binned spatial sampling ranging from 3 to 5 km, while the high spectral resolution "HR" channel ranges from 205 to 235 nm at a 0.2 nm spectral resolution and a binned spatial sampling ranging from 12 to 24 km. The spectral overlap between LR and HR channels ensures a proper cross-calibration of the more SNR-challenging HR channel on the simulateneously acquired LR baseline. This is especially welcome since this overlap occurs in the spectral range most sensitive to our main target gaseous species (SO_2 and SO).

Each channel consists of an entrance baffle, an objective composed of two lenses and a stop diaphragm, and a spectrometer composed of a slit and a toroidal holographic grating. It also comprises a shortpass filter to reject the wavelengths above the higher limit of the bands (> 240 nm for HR, > 380 nm for LR) and a zero-order trap to avoid straylight that may be due to internal reflections of the grating zero-order (only the first diffraction order is used). The optical layout is presented in Fig. 6. Both LR and HR slits are parallel and the optical layout is such that both channels have the same instantaneous field of view. Each slit image is then spectrally dispersed by its respective toroidal holographic grating and is focused on a shared (for cost reasons) CMOS back-side illuminated detector. The spectra of LR and HR channels are dispersed one above the other on the same focal plane (Fig. 7), with very little cross-contamination between both channels.

The VenSpec-U instrument includes two electronic assemblies:

- a Main Electronics unit, composed itself of a power conversion board, a data processing board, and an interface board in charge of the electrical and data interface with the subsystems and housekeeping conditioning;

Table 1
Science Traceability Matrix for VeSUV.

Science Objective	*Requirement*	*Reference*
SO_2		
Observing SO_2	spectral range including 190–320 nm	Marcq et al. (2020)
SO_2 precision $< 10\%$	SNR(250nm) > 200 at 1 nm sampling **and** SO:SO_2 precision $< 25\%$	this paper
SO		
Observing SO	spectral range including 205–235 nm	Phillips (1981)
Separating SO & SO_2	spectral sampling < 0.5 nm	Jessup et al. (2015)
SO:SO_2 precision $< 25\%$	SNR(250nm) > 100 at 0.2 nm sampling	this paper
UV absorber & clouds		
Constraining UV absorber composition	spectral range extending > 365 nm	Pérez-Hoyos et al. (2018)
Resolving small-scale convection	spatial sampling < 5 km	Titov et al. (2008)
Constraining droplet properties	transverse angular FoV $> 20°$	Markiewicz et al. (2018)
All investigations		
4+ observations over same fixed spot relatively to surface	transverse spatial FoV > 100 km	Kouyama et al. (2017)
Representative data set for cloud top climatology	coverage $> 60\%$ with each gap $< 10\%$ (wrt. lat., long., loc. time)	

Table 2
VenSpec-U instrument design summary (Current best estimates).

Optical objectives	2 aspherical lenses, telecentric in image space	
Focal length	22.9 mm	
Angular FoV	22.5°	
Aperture	∅4.1 mm	∅2.04 mm
Spectrometer	**LR**	**HR**
Spectral range	190–380 nm	205–235 nm
Spectral resolution	2 nm	0.2 nm
Arms length	200 mm	200 mm
Slit size	9 mm ×180 μm	9 mm ×126 μm
Spatial magnification	1	1
Grating ruling density	500 gr/mm	3110 gr/mm
Dispersion	9.5 nm/mm	1.5 nm/mm
Detector		
Physical size	20.48 mm × 20.48 mm	
Number of (unbinned) pixels	2048 × 2048	
Operating temperature	≈ 250 K	
Physical characteristics		
Mass	6.8 kg including maturity margin	
Power	6.5 to 18.7 W	
Dimensions	250 × 280 × 290 mm^3	

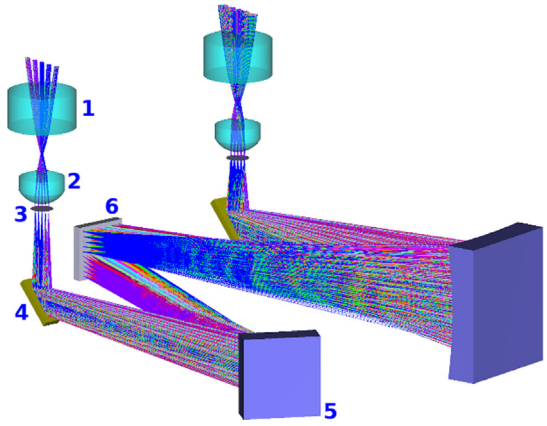

Fig. 6. VenSpec-U optical layout overview, with the HR and LR channels respectively on the left and on the right. For the HR channel: (1) Front lens; (2) Rear lens; (3) Slit; (4) Reflective filter; (5) Grating; (6) Shared sensor.

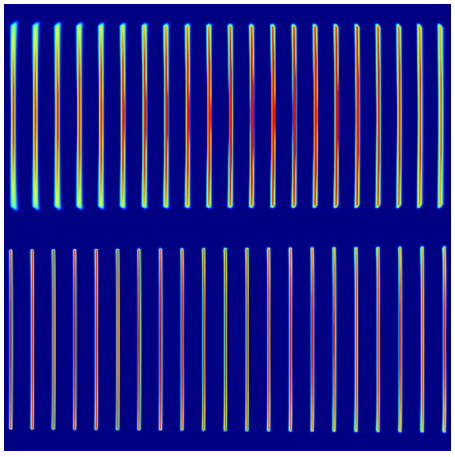

Fig. 7. VenSpec-U focal plane shared between the LR (top) and HR (bottom) channels, showing both slit images at regularly 21 spaced wavelengths covering their respective spectral ranges. The long axis of both slits provide spatial information, whereas the spectral dispersion takes place along the short axis of both slits.

– a detector frontend electronics.

The Main Electronics relies on a hybrid hardware/software mix to allow for flexibility and maintainability thanks to the software, and timing performances thanks to the hardware. The data processing board is controlled by a FPGA based on the NanoXplore architecture which offers on-ground reprogrammability while having intrinsically good immunity to radiations. The most recent values of several key instrumenal characteristics are displayed in Table 2.

4.2. Interfaces and resource requirements

Fig. 8 shows the block diagram presenting the internal and external interfaces of the instrument and its subsystems.

Interfaces between VenSpec-U and spacecraft are: (1) Thermal interface providing a cold finger to cool down the detector and a thermal reference point for the electrical box and the optical bench; (2) Power interface (redundant 28 V) to VenSpec-U electronics and spacecraft controlled heaters and (3) Data SpaceWire link (including ground debug EGSE). Commanding, data link to the spacecraft and power supply will be provided by a dedicated Central Control Unit (CCU). The instrument mass including maturity margin is 6.8 kg. The power resources are 6.5 W in standby mode, 13.2 W during science observation, and 18.7 W for peak power. The data rate ranges from 76 to 644 kbit/s depending on the distance to the clouds and on the spatial sampling mode.

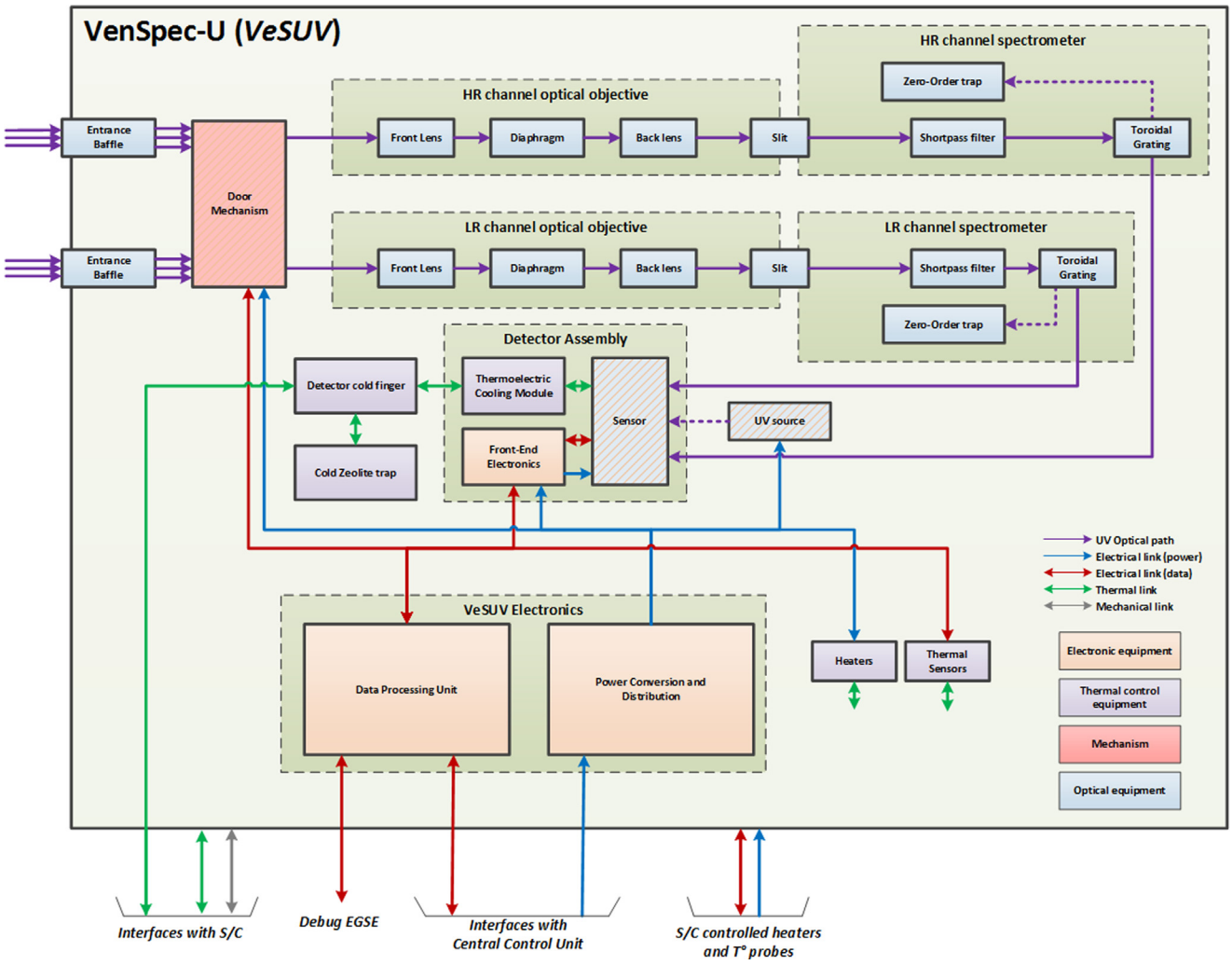

Fig. 8. VenSpec-U block diagram.

4.3. Observing strategy

As previously mentioned in Section 3.1.3, VenSpec-U nominal science operations on day side consist of four consecutive sessions of dayside observations lasting about 50 min each. Since the polar orbit slowly precess relatively to the surface, there is significant overlapping between these consecutive observations, allowing for a hourly timescale study of any atmospheric features that would fixed relatively to the surface. These observations are interleaved with star, internal and dark calibrations performed once or twice per month on the night side.

The identical instantaneous field of view of the two channels allows simultaneous observations of the same target as well as simultaneous calibrations on the same star. The narrow-slit axis of the detector contains the spectral information, whereas the long-slit axis contains the spatial information along the 22.5° field of view of each slit. The remaining spatial direction is provided through orbital scrolling, an observational strategy known as "pushbroom". Observations can be conducted in strict nadir or near-nadir (emission angle $< 30°$) geometries.

Binning on the spatial axis is performed on the detector, enabling a SNR higher than 100 for the HR channel and 200 for the LR one (resulting in a coarser spatial sampling on the more dispersed HR channel). The detector will be controlled such that the integration time, the binning scheme and frame stacking are adjusted independently (and simultaneously) for each channel, giving high flexibility and providing parameters for the optimisation of each science acquisition (SNR vs. angular sampling vs. distance between the instrument and the cloud top vs. etc.). The SNR objectives are reached for a spatial sampling always smaller than 5 km on the LR channel, insuring the sufficient spatial resolution to investigate the cloud top convective processes at less than 10 km length scale (Section 3.2). For the HR channel, the higher spectral resolution and lower radiance below 240 nm prevents any access to the 10 km length scale, so that our best effort while meeting the SNR objective yields a spatial sampling between 12 and 24 km depending on the observation.

Based on the analysis shown in Section 3.3, such SNR and spectral resolution should allow for a determination of the SO:SO_2 ratio with an accuracy better than 25% using

the HR channel, and of the total $SO + SO_2$ column with an accuracy better than 10%. In both cases, this will result in a significant improvement compared to the accuracy of past measurements discussed in Section 2.1. Incidentally, these SNR and spectral resolution values also yield measurements of unknown UV absorber (through its imaginary refractive index) and cloud top altitude with respective accuracies of $\sim 10\%$ and ~ 200 m, much improved compared to e.g. SPICAV-UV retrievals.

4.4. Additional measurement capabilities

Aside from its core science objectives, this instrument may incidentally measure other properties of the upper atmosphere, either through reflected solar light on the day side or aeronomic emissions on the night side.

4.4.1. Other gaseous species

Using the radiative transfer model described in Section 3.3.1 with the instrumental SNR and spectral resolution, we were also able to compute the sensitivity of the instrument to other UV absorbing trace species that exist (or may exist) at or above Venus cloud top, using the same methodology as described in Section 3.3, assuming nadir viewing over typical dayside conditions. Sensitivity variations with e.g. SO_2 content or haze variability should be moderate considering the climatogical range already observed by e.g. SPICAV-UV (Marcq et al., 2020).

- O_3 Ozone should be detectable using the LR channel in nadir viewing mode, provided its mixing ratio is more than a few ppbv at cloud top; this is about one order of magnitude improvement from the SPICAV detection at higher latitudes (Marcq et al., 2019) and may allow tracking of O_3 at lower latitudes, thus better constraining coupled chemical transport and photochemistry models.
- ClO Chlorine monoxide is an expected product from chlorine photochemistry above the clouds (Mills and Allen, 2007; Zhang et al., 2012), which is thought to interact with sulphur photochemistry in the mesosphere above the clouds. We predict a sensitivity threshold to ClO at about 10 ppbv between 85 and 95 km where ClO mixing ratio should be peaking. This is about one ordre of magnitude larger than average model predictions, so that ClO detection is unlikely but not impossible in favourable circumstances.
- PH_3 Following the claims of about 20 ppb of phosphine within Venus' clouds (Greaves et al., 2020), we also investigated our sensitivity to this species, which presents an absorption band near 180 nm. Considering the very low signal at these wavelengths, we predict a very weak sensitivity to PH_3 in the 50–70 km altitude range, over 100 ppb. We therefore advise that remote sensing confirmation or invalidation of PH_3 presence in Venus' clouds should rather be performed in the thermal IR range near 10 μm (Encrenaz et al., 2020b).

4.4.2. Large scale atmospheric dynamics

Due to the low orbit of *EnVision*, even a field-of-view in excess of 20° does not cover a large transverse distance projected at cloud top (on the order of 100 to 200 km). Therefore, due to the zonal superrotation, the UV cloud contrasts observed during one orbit will have shifted westwards by several hundreds of kilometers when the orbiter comes back during the next orbit, and these constrasts will have left the field of view. This makes cloud tracking not possible with the current orbit and instrument design, except for latitudes higher than about 70° where the superrotation is significantly slower than at lower latitudes. Even there, the relatively low SNR due to the high solar zenith angles prevailing near the poles could be challenging. Nevertheless, if some cloud tracking were possible, the spectroscopic capabilities of VeSUV could yield interesting results if the retrieved vector speed would differ with wavelength, as evidenced with UVI by Horinouchi et al. (2018).

Also, although wind determination by feature tracking will not be possible in general, EnVision's regular coverage will enable other types of investigations relevant to large-scale dynamics, e.g. monitoring of the latitudinal extent of the UV-bright clouds typically present at Venus' poles, and monitoring of long-term variations in UV albedo, which may be linked to long-period atmopsheric dynamical cycles (Lee et al., 2019).

4.4.3. Night side observations

Stellar occultations at a monthly interval are essential for the instrumental calibration. Such occultations, with a line-of-sight to the star ingressing or egressing out of the atmosphere, may also provide vertically resolved observations of the mesospheric extinction (due to both particulate matter and gaseous species), like SPICAV-UV performed in its nominal science case. A thorough knowledge of EnVision's orbit and pointing on Venus' night side would be required first in order to assess the achievable accuracy, vertical resolution and coverage with respect to latitude, local solar time and altitude range.

In the same observational geometry, limb observations of Venus could also be acquired. This would in principle allow for aeronomical studies of the upper mesosphere, since e.g. VeSUV's spectral range encompasses both δ (190–240 nm) and γ (255–270 nm) bands of nitric oxide (NO) airglow (Gérard et al., 2008; Stiepen et al., 2013; Royer et al., 2016). However, the very weak intensity of the airglows compared to the solar radiation backscattered on the day side (which is the primary target and main radiometric design driver for VeSUV optical conception) would require very long integration times and/or extensive spatial binning in order to reach a workable SNR, thereby

hampering severely the spatial resolution of such observations. Furthermore, current science operation scenario does not allow for VenSpec-U operating on the night side except for calibration purposes (about once a month), so that the spatial and temporal coverage would be modest. Nevertheless, we intend to study more in detail the feasibility of such aeronomical observations for an extended science case if EnVision were selected.

4.4.4. Ultra high spatial resolution mode

With the required spectral resolution of 2 nm, a satisfactory SNR can only be reached for a spatial sampling larger than 3 km even in optimal conditions. Unfortunately, some dynamical phenomena e.g. gravity waves (Piccialli et al., 2014), or fine scale convection are known to occur at a sub-km range. We may tentatively investigate these ultra-short horizontal scales, provided we perform a trade-off between spectral binning/resolution (which is not too stringent for UV absorber measurements at the expense of gaseous spectroscopy) and spatial/temporal binning. This ultra-high spatial observations campaigns may occur over known targets where coupling between surface topography and gravity waves is known to take place. However, these would amount to a small proportion of VeSUV observations if we want to achieve our global coverage of SO and SO_2 measurements, as well as keeping data rate below our global allocation on board the spacecraft (936 Mbit per orbit as of January 2021).

5. Conclusion

We have shown here that it is indeed possible to build, with existing (or currently in development) technology, a two-channel UV spectral imager onboard a Venus orbiter that would allow for significant improvements compared with previous UV measurements of sulphur-bearing gases, cloud UV albedo and altitude. The improvement factors range from about 2 for SO_2 abundance up to about 10 for SO:SO_2 ratio. Incidentally, other interesting measurements could be obtained during the occultations of calibration stars through the Venusian mesosphere to derive constraints of the vertical profiles of gaseous and particulate species above the clouds. Also, glory observations would allow us to retrieve microphysical properties of cloud aerosols, so that the complex interactive process of photochemistry (Shao et al., 2020) and cloud aerosol formation (McGouldrick, 2017) could be analyzed comprehensively.

The scientific potential of the VeSUV instrument is significant on its own. When the instrument is coupled with e.g. simultaneous and horizontally co-located high resolution day side or night side infrared spectroscopy, numerous other gaseous species (carbon monoxide, water vapor, carbonyl sulphide, hydrogen halides) can be measured over a broad altitude range, allowing for a more comprehensive assessment of the interplay between photochemistry and atmospheric dynamics at the cloud top of Venus, as well as any links between those processes and any active volcanism at the surface. The proposed ESA M5 mission concept *EnVision*, which proposes to include the spectrometer suite *VenSpec* including a multispectral infrared surface imager (Helbert et al., 2016), a high-resolution infrared spectrometer and our proposed UV instrument, would be ideally suited to accomplish these tasks.

Declaration of Competing Interest

The authors declare that they have no conflict of interest.

Acknowledgements

The development of the VenSpec-U experiment onboard the EnVision mission is an activity carried out under a programme of the European Space Agency. The activity is supported and funded by the European Space Agency (ESA), the French space agency (CNES), the French national centre for scientific research (CNRS), the University of Versailles Saint Quentin (UVSQ, France) and Sorbonne University (SU, France). The view expressed in this publication does not reflect the official opinion of the supporting and funding agencies. CFW acknowledges funding from the UK Space Agency grant ST/V003224/1. YJL has received funding from EU Horizon 2020 MSCA-IF N° 841432.

The UVI data we processed in Section 3.2.1 can be accessed at the following DOIs. For Level 2 data: Murakami, S., M. Yamada, A. Yamazaki, K. McGouldrick, Y. Yamamoto, G. L. Hashimoto, Venus Climate Orbiter Akatsuki UVI Calibrated Data v1.0, VCO-V-UVI-3-CDR-V1.0, NASA Planetary Data System, DOI:10.17597/ISAS.DARTS/VCO-00003, 2018. For geometry data: Murakami, S., M. Yamada, K. McGouldrick, Y. Yamamoto, G. L. Hashimoto, Venus Climate Orbiter Akatsuki UVI Geometry Information v1.0, VCO-V-UVI-3-SEDR-V1.0, NASA Planetary Data System, DOI:10.17597/ISAS.DARTS/VCO-00004, 2018.

We also want to acknowledge the Crystal IS company, which has graciously provided us with ultraviolet leds for technical assessment.

We finally wish to thank the two anonymous reviewers for their helpful comments resulting in a much improved version of this work.

References

Arney, G., Meadows, V., Crisp, D., Schmidt, S.J., Bailey, J., Robinson, T., 2014. Spatially resolved measurements of H_2O, HCl, CO, OCS, SO_2, cloud opacity, and acid concentration in the Venus near-infrared spectral windows. J. Geophys. Res. (Planets) 119, 1860–1891. https://doi.org/10.1002/2014JE004662.

Barker, E.S., 1979. Detection of SO_2 in the UV spectrum of Venus. Geophys. Res. Lett. 6, 117–120. https://doi.org/10.1029/GL006i002p00117.

Barstow, J.K., Tsang, C.C.C., Wilson, C.F., Irwin, P.G.J., Taylor, F.W., McGouldrick, K., Drossart, P., Piccioni, G., Tellmann, S., 2012. Models of the global cloud structure on Venus derived from Venus Express observations. Icarus 217, 542–560. https://doi.org/10.1016/j.icarus.2011.05.018.

Bertaux, J.L., Nevejans, D., Korablev, O., Villard, E., Quémerais, E., Neefs, E., Montmessin, F., Leblanc, F., Dubois, J.P., Dimarellis, E., Hauchecorne, A., Lefèvre, F., Rannou, P., Chaufray, J.Y., Cabane, M., Cernogora, G., Souchon, G., Semelin, F., Reberac, A., van Ransbeek, E., Berkenbosch, S., Clairquin, R., Muller, C., Forget, F., Hourdin, F., Talagrand, O., Rodin, A., Fedorova, A., Stepanov, A., Vinogradov, I., Kiselev, A., Kalinnikov, Y., Durry, G., Sandel, B., Stern, A., Gérard, J.C., 2007. SPICAV on Venus Express: Three spectrometers to study the global structure and composition of the Venus atmosphere. Plan Space Sci. 55, 1673–1700. https://doi.org/10.1016/j.pss.2007.01.016.

Braak, C.J., de Haan, J.F., Hovenier, J.W., Travis, L.D., 2002. Spatial and temporal variations of Venus haze properties obtained from Pioneer Venus Orbiter polarimetry. J. Geophys. Res. (Planets) 107 (E5), 5029. https://doi.org/10.1029/2001JE001502.

Dollfus, A., Boyer, C., Camichel, H., 1960. Commission des surfaces planétaires: Étude photographique de Vénus en lumière violette et ultra-violette. L'Astronomie 74, 375.

Drossart, P., Piccioni, G., Adriani, A., Angrilli, F., Arnold, G., Baines, K. H., Bellucci, G., Benkhoff, J., Bézard, B., Bibring, J.P., Blanco, A., Blecka, M.I., Carlson, R.W., Coradini, A., Di Lellis, A., Encrenaz, T., Erard, S., Fonti, S., Formisano, V., Fouchet, T., Garcia, R., Haus, R., Helbert, J., Ignatiev, N.I., Irwin, P.G.J., Langevin, Y., Lebonnois, S., Lopez-Valverde, M.A., Luz, D., Marinangeli, L., Orofino, V., Rodin, A.V., Roos-Serote, M.C., Saggin, B., Sanchez-Lavega, A., Stam, D. M., Taylor, F.W., Titov, D., Visconti, G., Zambelli, M., Hueso, R., Tsang, C.C.C., Wilson, C.F., Afanasenko, T.Z., 2007. Scientific goals for the observation of Venus by VIRTIS on ESA/Venus express mission. Planet. Space Sci. 55 (12), 1653–1672. https://doi.org/10.1016/j.pss.2007.01.003.

Encrenaz, T., Greathouse, T.K., Roe, H., Richter, M., Lacy, J., Bézard, B., Fouchet, T., Widemann, T., 2012. HDO and SO_2 thermal mapping on Venus: evidence for strong SO_2 variability. A&A 543, A153. https://doi.org/10.1051/0004-6361/201219419.

Encrenaz, T., Greathouse, T.K., Richter, M.J., Lacy, J., Widemann, T., Bézard, B., Fouchet, T., deWitt, C., Atreya, S.K., 2013. HDO and SO_2 thermal mapping on Venus. II. The SO_2 spatial distribution above and within the clouds. A&A 559 (A65). https://doi.org/10.1051/0004-6361/201322264.

Encrenaz, T., Greathouse, T.K., Richter, M.J., DeWitt, C., Widemann, T., Bézard, B., Fouchet, T., Atreya, S.K., Sagawa, H., 2016. HDO and SO_2 thermal mapping on Venus. III. Short-term and long-term variations between 2012 and 2016. A&A 595, A74. https://doi.org/10.1051/0004-6361/201628999.

Encrenaz, T., Greathouse, T.K., Marcq, E., Sagawa, H., Widemann, T., Bézard, B., Fouchet, T., Lefèvre, F., Lebonnois, S., Atreya, S.K., Lee, Y.J., Giles, R., Watanabe, S., 2019. HDO and SO_2 thermal mapping on Venus. IV. Statistical analysis of the SO_2 plumes. A&A 623 (A70). https://doi.org/10.1051/0004-6361/201833511.

Encrenaz, T., Greathouse, T.K., Marcq, E., Sagawa, H., Widemann, T., Bézard, B., Fouchet, T., Lefèvre, F., Lebonnois, S., Atreya, S.K., Lee, Y.J., Giles, R., Watanabe, S,. Shao, W., Zhang, X., Bierson, C.J., 2020a HDO and SO_2 thermal mapping on Venus. V. Evidence for a long-term anti-correlation. A&A 639, A69, doi:10.1051/0004-6361/202037741.

Encrenaz, T., Greathouse, T.K., Marcq, E., Widemann, T., Bézard, B., Fouchet, T., Giles, R., Sagawa, H., Greaves, J., Sousa-Silva, C., 2020b. A stringent upper limit of the PH_3 abundance at the cloud top of Venus. A&A 643, L5, 10.1051/0004-6361/202039559, 2010.07817.

Esposito, L.W., 1984. Sulfur dioxide - Episodic injection shows evidence for active Venus volcanism. Science 223, 1072–1074. https://doi.org/10.1126/science.223.4640.1072.

Esposito, L.W., Winick, J.R., Stewart, A.I., 1979. Sulfur dioxide in the Venus atmosphere - Distribution and implications. Geophys. Res. Lett. 6, 601–604. https://doi.org/10.1029/GL006i007p00601.

Esposito, L.W., Copley, M., Eckert, R., Gates, L., Stewart, A.I.F., Worden, H., 1988. Sulfur dioxide at the Venus cloud tops, 1978–1986. J. Geophys. Res. 93, 5267–5276. https://doi.org/10.1029/JD093iD05p05267.

Frandsen, B.N., Wennberg, P.O., Kjaergaard, H.G., 2016. Identification of OSSO as a near-UV absorber in the Venusian atmosphere. Geophys. Res. Lett. 43 (21), 11,146–11,155. https://doi.org/10.1002/2016GL070916.

Frandsen, B.N., Farahani, S., Vogt, E., Lane, J.R., Kjaergaard, H.G., 2020. Spectroscopy of OSSO and Other Sulfur Compounds Thought to be Present in the Venus Atmosphere. J. Phys. Chem. A 124 (35), 7047–7059. https://doi.org/10.1021/acs.jpca.0c04388.

Fukuhara, T., Futaguchi, M., Hashimoto, G.L., Horinouchi, T., Imamura, T., Iwagaimi, N., Kouyama, T., Murakami, S.Y., Nakamura, M., Ogohara, K., Sato, M., Sato, T.M., Suzuki, M., Taguchi, M., Takagi, S., Ueno, M., Watanabe, S., Yamada, M., Yamazaki, A., 2017. Large stationary gravity wave in the atmosphere of Venus. Nat. Geosci. 10 (2), 85–88. https://doi.org/10.1038/ngeo2873.

García Muñoz, A., Pérez-Hoyos, S., Sánchez-Lavega, A., 2014. Glory revealed in disk-integrated photometry of Venus. A&A 566, L1. https://doi.org/10.1051/0004-6361/201423531, 1406.0277.

Gérard, J.C., Cox, C., Saglam, A., Bertaux, J.L., Villard, E., Nehmé, C., 2008. Limb observations of the ultraviolet nitric oxide nightglow with SPICAV on board Venus Express. J. Geophys. Res. (Planets) 113 (9), E00B03. https://doi.org/10.1029/2008JE003078.

Ghail R, Wilson C, Widemann T, Bruzzone L, Dumoulin C, Helbert J, Herrick R, Marcq E, Mason P, Rosenblatt P, Vandaele AC, Burtz LJ (2017) Envision: understanding why our most earth-like neighbour is so different. 1703.09010.

Greaves, J.S., Richards, A.M.S., Bains, W., Rimmer, P.B., Sagawa, H., Clements, D.L., Seager, S., Petkowski, J.J., Sousa-Silva, C., Ranjan, S., Drabek-Maunder, E., Fraser, H.J., Cartwright, A., Mueller-Wodarg, I., Zhan, Z., Friberg, P., Coulson, I., Lee, E., Hoge, J., 2020. Phosphine gas in the cloud decks of Venus. Nature Astronomy, 10.1038/s41550-020-1174-4, 2009.06593.

Hapke, B., Nelson, R., 1975. Evidence for an elemental sulfur component of the clouds from Venus spectrophotometry. J. Atmospheric Sci. 32, 1212–1218. https://doi.org/10.1175/1520-0469(1975)032<1212:EFAESC>2.0.CO;2.

Hartley, K.K., Wolff, A.R., Travis, L.D., 1989. Croconic acid: An absorber in the Venus clouds?. Icarus 77 (2), 382–390. https://doi.org/10.1016/0019-1035(89)90095-X.

Haus, R., Kappel, D., Tellmann, S., Arnold, G., Piccioni, G., Drossart, P., Häusler, B., 2016. Radiative energy balance of Venus based on improved models of the middle and lower atmosphere. Icarus 272, 178–205. https://doi.org/10.1016/j.icarus.2016.02.048.

Helbert, J., Wendler, D., Walter, I., Widemann, T., Marcq, E., Guignan, G., Ferrari, S., Maturilli, A., Mueller, N., Kappel, D., et al., 2016. The venus emissivity mapper (vem) concept. Infrared Remote Sensing and Instrumentation XXIV, vol 9973. International Society for Optics and Photonics, p. 99730R.

Helbert, J., Vandaele, A.C., Marcq, E., Robert, S., Ryan, C., Guignan, G., Rosas-Ortiz, Y., Neefs, E., Thomas, I.R., Arnold, G., Peter, G., Widemann, T., Lara, L., 2019. The VenSpec suite on the ESA EnVision mission to Venus. In: Infrared Remote Sensing and Instrumentation XXVII, Society of Photo-Optical Instrumentation Engineers (SPIE) Conference Series, vol. 11128, p. 1112804, doi:10.1117/12.2529248.

Heyden, F.J., Kiess, C.C., Kiess, H.K., 1959. Spectrum of Venus in the Violet and Near-Ultraviolet. Science 130 (3383), 1195. https://doi.org/10.1126/science.130.3383.1195.

Horinouchi, T., Kouyama, T., Lee, Y.J., Sy, Murakami, Ogohara, K., Takagi, M., Imamura, T., Nakajima, K., Peralta, J., Yamazaki, A., Yamada, M., Watanabe, S., 2018. Mean winds at the cloud top of

Venus obtained from two-wavelength UV imaging by Akatsuki. Earth, Planets, Space 70 (1), 10. https://doi.org/10.1186/s40623-017-0775-3.

Hueso, R., Peralta, J., Sánchez-Lavega, A., 2012. Assessing the long-term variability of Venus winds at cloud level from VIRTIS-Venus Express. Icarus 217, 585–598. https://doi.org/10.1016/j.icarus.2011.04.020.

Hueso, R., Peralta, J., Garate-Lopez, I., Bandos, T., Snchez-Lavega, A., 2015. Six years of venus winds at the upper cloud level from uv, visible and near infrared observations from virtis on venus express. Planet. Space Sci. 113–114, 78–99. https://doi.org/10.1016/j.pss.2014.12.010, URL http://www.sciencedirect.com/science/article/pii/S0032063314004024, sI: Exploration of Venus.

Imamura, T., Higuchi, T., Maejima, Y., Takagi, M., Sugimoto, N., Ikeda, K., Ando, H., 2014. Inverse insolation dependence of Venus' cloud-level convection. Icarus 228, 181–188. https://doi.org/10.1016/j.icarus.2013.10.012.

Jessup, K.L., Marcq, E., Mills, F., Mahieux, A., Limaye, S., Wilson, C., Allen, M., Bertaux, J.L., Markiewicz, W., Roman, T., Vandaele, A.C., Wilquet, V., Yung, Y., 2015. Coordinated Hubble Space Telescope and Venus Express Observations of Venus' upper cloud deck. Icarus 258, 309–336. https://doi.org/10.1016/j.icarus.2015.05.027.

Kawabata, K., Coffeen, D.L., Hansen, J.E., Lane, W.A., Sato, M., Travis, L.D., 1980. Cloud and haze properties from Pioneer Venus polarimetry. J. Geophys. Res. 85, 8129–8140. https://doi.org/10.1029/JA085iA13p08129.

Khatuntsev, I.V., Patsaeva, M.V., Titov, D.V., Ignatiev, N.I., Turin, A.V., Limaye, S.S., Markiewicz, W.J., Almeida, M., Roatsch, T., Moissl, R., 2013. Cloud level winds from the Venus Express Monitoring Camera imaging. Icarus 226, 140–158. https://doi.org/10.1016/j.icarus.2013.05.018.

Kitahara, T., Imamura, T., Sato, T.M., Yamazaki, A., Lee, Y.J., Yamada, M., Watanabe, S., Taguchi, M., Fukuhara, T., Kouyama, T., Sy, Murakami, Hashimoto, G.L., Ogohara, K., Kashimura, H., Horinouchi, T., Takagi, M., 2019. Stationary Features at the Cloud Top of Venus Observed by Ultraviolet Imager Onboard Akatsuki. J. Geophys. Res. (Planets) 124 (5), 1266–1281. https://doi.org/10.1029/2018JE005842.

Knibbe, W.J.J., de Haan, J.F., Hovenier, J.W., Travis, L.D., 1998. Analysis of temporal variations of the polarization of Venus observed by Pioneer Venus Orbiter. J. Geophys. Res. 103 (E4), 8557–8574. https://doi.org/10.1029/97JE03558.

Kouyama, T., Imamura, T., Taguchi, M., Fukuhara, T., Sato, T.M., Yamazaki, A., Futaguchi, M., Murakami, S., Hashimoto, G.L., Ueno, M., Iwagami, N., Takagi, S., Takagi, M., Ogohara, K., Kashimura, H., Horinouchi, T., Sato, N., Yamada, M., Yamamoto, Y., Ohtsuki, S., Sugiyama, K., Ando, H., Takamura, M., Yamada, T., Satoh, T., Nakamura, M., 2017. Topographical and Local Time Dependence of Large Stationary Gravity Waves Observed at the Cloud Top of Venus. Geophys. Res. Lett. 44 (24), 12,098–12,105. https://doi.org/10.1002/2017GL075792.

Krasnopolsky, V.A., 2017. On the iron chloride aerosol in the clouds of Venus. Icarus 286, 134–137. https://doi.org/10.1016/j.icarus.2016.10.003.

Lee, Y.J., Imamura, T., Schröder, S.E., Marcq, E., 2015. Long-term variations of the UV contrast on Venus observed by the Venus Monitoring Camera on board Venus Express. Icarus 253, 1–15. https://doi.org/10.1016/j.icarus.2015.02.015.

Lee, Y.J., Yamazaki, A., Imamura, T., Yamada, M., Watanabe, S., Sato, T.M., Ogohara, K., Hashimoto, G.L., Murakami, S., 2017. Scattering Properties of the Venusian Clouds Observed by the UV Imager on board Akatsuki. AJ 154 (2), 44. https://doi.org/10.3847/1538-3881/aa78a5.

Lee, Y.J., Jessup, K.L., Perez-Hoyos, S., Titov, D.V., Lebonnois, S., Peralta, J., Horinouchi, T., Imamura, T., Limaye, S., Marcq, E., Takagi, M., Yamazaki, A., Yamada, M., Watanabe, S., Sy, Murakami, Ogohara, K., McClintock, W.M., Holsclaw, G., Roman, A., 2019. Long-term Variations of Venus's 365 nm Albedo Observed by Venus Express, Akatsuki, MESSENGER, and the Hubble Space Telescope. AJ 158 (3), 126. https://doi.org/10.3847/1538-3881/ab3120, 1907.09683.

Lee, Y.J., García Muñoz, A., Imamura, T., Yamada, M., Satoh, T., Yamazaki, A., Watanabe, S., 2020. Brightness modulations of our nearest terrestrial planet Venus reveal atmospheric super-rotation rather than surface features. Nature Commun. 11, 5720, 10.1038/s41467-020-19385-6, 2011.09271.

Lefèvre, M., Spiga, A., Lebonnois, S., 2017. Three-dimensional turbulence-resolving modeling of the Venusian cloud layer and induced gravity waves. J. Geophys. Res. (Planets) 122 (1), 134–149. https://doi.org/10.1002/2016JE005146.

Lefèvre, M., Lebonnois, S., Spiga, A., 2018. Three-Dimensional Turbulence-Resolving Modeling of the Venusian Cloud Layer and Induced Gravity Waves: Inclusion of Complete Radiative Transfer and Wind Shear. J. Geophys. Res. (Planets) 123 (10), 2773–2789. https://doi.org/10.1029/2018JE005679.

Lefèvre, M., Spiga, A., Lebonnois, S., 2020. Mesoscale modeling of Venus' bow-shape waves. Icarus 335, 113376, 10.1016/j.icarus.2019.07.010, 1902.07010.

Limaye, S.S., Mogul, R., Smith, D.J., Ansari, A.H., Słowik, G.P., Vaishampayan, P., 2018. Venus' Spectral Signatures and the Potential for Life in the Clouds. Astrobiology 18 (9), 1181–1198. https://doi.org/10.1089/ast.2017.1783.

Marcq, E., Belyaev, D., Montmessin, F., Fedorova, A., Bertaux, J.L., Vandaele, A.C., Neefs, E., 2011. An investigation of the SO_2 content of the venusian mesosphere using SPICAV-UV in nadir mode. Icarus 211, 58–69. https://doi.org/10.1016/j.icarus.2010.08.021.

Marcq, E., Bertaux, J.L., Montmessin, F., Belyaev, D., 2013. Variations of sulphur dioxide at the cloud top of Venus's dynamic atmosphere. Nature Geosci. 6 (1), 25–28. https://doi.org/10.1038/ngeo1650, URL http://hal.archives-ouvertes.fr/hal-00767475.

Marcq, E., Baggio, L., Lefèvre, F., Stolzenbach, A., Montmessin, F., Belyaev, D., Korablev, O., Bertaux, J.L., 2019. Discovery of cloud top ozone on Venus. Icarus 319, 491–498. https://doi.org/10.1016/j.icarus.2018.10.006.

Marcq, E., Lea Jessup, K., Baggio, L., Encrenaz, T., Lee, Y.J., Montmessin, F., Belyaev, D., Korablev, O., Bertaux, J.L., 2020. Climatology of SO_2 and UV absorber at Venus' cloud top from SPICAV-UV nadir dataset. Icarus 335, 113368. https://doi.org/10.1016/j.icarus.2019.07.002.

Markiewicz, W.J., Titov, D.V., Ignatiev, N., Keller, H.U., Crisp, D., Limaye, S.S., Jaumann, R., Moissl, R., Thomas, N., Esposito, L., Watanabe, S., Fiethe, B., Behnke, T., Szemerey, I., Michalik, H., Perplies, H., Wedemeier, M., Sebastian, I., Boogaerts, W., Hviid, S.F., Dierker, C., Osterloh, B., Böker, W., Koch, M., Michaelis, H., Belyaev, D., Dannenberg, A., Tschimmel, M., Russo, P., Roatsch, T., Matz, K.D., 2007. Venus Monitoring Camera for Venus Express. Planet. Space Sci. 55 (12), 1701–1711. https://doi.org/10.1016/j.pss.2007.01.004.

Markiewicz, W.J., Petrova, E., Shalygina, O., Almeida, M., Titov, D.V., Limaye, S.S., Ignatiev, N., Roatsch, T., Matz, K.D., 2014. Glory on Venus cloud tops and the unknown UV absorber. Icarus 234, 200–203. https://doi.org/10.1016/j.icarus.2014.01.030.

Markiewicz, W.J., Petrova, E.V., Shalygina, O.S., 2018. Aerosol properties in the upper clouds of Venus from glory observations by the Venus Monitoring Camera (Venus Express mission). Icarus 299, 272–293. https://doi.org/10.1016/j.icarus.2017.08.011.

McGouldrick, K., 2017. Effects of variation in coagulation and photochemistry parameters on the particle size distributions in the Venus clouds. Earth, Planets, Space 69 (1), 161. https://doi.org/10.1186/s40623-017-0744-x.

Mills, F.P., Allen, M., 2007. A review of selected issues concerning the chemistry in Venus' middle atmosphere. Planet. Space Sci. 55, 1729–1740. https://doi.org/10.1016/j.pss.2007.01.012.

Molaverdikhani, K., McGouldrick, K., Esposito, L.W., 2012. The abundance and vertical distribution of the unknown ultraviolet absorber in the venusian atmosphere from analysis of Venus Moni-

toring Camera images. Icarus 217, 648–660. https://doi.org/10.1016/j.icarus.2011.08.008.

Montmessin, F., Bertaux, J.L., Lefèvre, F., Marcq, E., Belyaev, D., Gérard, J.C., Korablev, O., Fedorova, A., Sarago, V., Vandaele, A.C., 2011. A layer of ozone detected in the nightside upper atmosphere of Venus. Icarus 216, 82–85. https://doi.org/10.1016/j.icarus.2011.08.010.

Na, C.Y., Esposito, L.W., Skinner, T.E., 1990. International Ultraviolet Explorer observations of Venus SO_2 and SO. J. Geophys. Res. 95, 7485–7491. https://doi.org/10.1029/JD095iD06p07485.

Na, C.Y., Esposito, L.W., McClintock, W.E., Barth, C.A., 1994. Sulfur dioxide in the atmosphere of Venus. 2: Modeling results. Icarus 112, 389–395. https://doi.org/10.1006/icar.1994.1193.

Nakamura, M., Imamura, T., Ishii, N., Abe, T., Kawakatsu, Y., Hirose, C., Satoh, T., Suzuki, M., Ueno, M., Yamazaki, A., Iwagami, N., Watanabe, S., Taguchi, M., Fukuhara, T., Takahashi, Y., Yamada, M., Imai, M., Ohtsuki, S., Uemizu, K., Hashimoto, G.L., Takagi, M., Matsuda, Y., Ogohara, K., Sato, N., Kasaba, Y., Kouyama, T., Hirata, N., Nakamura, R., Yamamoto, Y., Horinouchi, T., Yamamoto, M., Hayashi, Y.Y., Kashimura, H., Ki, Sugiyama, Sakanoi, T., Ando, H., Sy, Murakami, Sato, T.M., Takagi, S., Nakajima, K., Peralta, J., Lee, Y.J., Nakatsuka, J., Ichikawa, T., Inoue, K., Toda, T., Toyota, H., Tachikawa, S., Narita, S., Hayashiyama, T., Hasegawa, A., Kamata, Y., 2016. AKATSUKI returns to Venus. Earth, Planets, Space 68 (1), 75. https://doi.org/10.1186/s40623-016-0457-6.

Navarro, T., Schubert, G., Lebonnois, S., 2018. Atmospheric mountain wave generation on Venus and its influence on the solid planet's rotation rate. Nat. Geosci. 11 (7), 487–491. https://doi.org/10.1038/s41561-018-0157-x.

Newville, M., Otten, R., Nelson, A., Ingargiola, A., Stensitzki, T., Allan, D., Fox, A., Carter, F., Michal, Pustakhod, D., et al., 2020. lmfit/lmfit-py. 1.0.1 doi:10.5281/zenodo.3814709.

Parkinson, W., 2003. Absolute absorption cross section measurements of CO_2 in the wavelength region 163–200 nm and the temperature dependence. Chem. Phys. 290, 251–256. https://doi.org/10.1016/S0301-0104(03)00146-0.

Peralta, J., Hueso, R., Sánchez-Lavega, A., Piccioni, G., Lanciano, O., Drossart, P., 2008. Characterization of mesoscale gravity waves in the upper and lower clouds of Venus from VEX-VIRTIS images. J. Geophys. Res. (Planets) 113:E00B18. https://doi.org/10.1029/2008JE003185.

Peralta, J., Hueso, R., Sánchez-Lavega, A., Lee, Y.J., Muñoz, A.G., Kouyama, T., Sagawa, H., Sato, T.M., Piccioni, G., Tellmann, S., Imamura, T., Satoh, T., 2017. Stationary waves and slowly moving features in the night upper clouds of Venus. Nature Astron. 1, 0187. https://doi.org/10.1038/s41550-017-0187, 1707.07796.

Pérez-Hoyos, S., Sánchez-Lavega, A., García-Muñoz, A., Irwin, P.G.J., Peralta, J., Holsclaw, G., McClintock, W.M., Sanz-Requena, J.F., 2018. Venus Upper Clouds and the UV Absorber From MESSENGER/MASCS Observations. J. Geophys. Res. (Planets) 123 (1), 145–162. https://doi.org/10.1002/2017JE005406, 1801.03820.

Petrova, E.V., Shalygina, O.S., Markiewicz, W.J., 2015a. The VMC/VEx photometry at small phase angles: Glory and the physical properties of particles in the upper cloud layer of Venus. Planet. Space Sci. 113, 120–134. https://doi.org/10.1016/j.pss.2014.11.013.

Petrova, E.V., Shalygina, O.S., Markiewicz, W.J., 2015b. UV contrasts and microphysical properties of the upper clouds of Venus from the UV and NIR VMC/VEx images. Icarus 260, 190–204. https://doi.org/10.1016/j.icarus.2015.07.015.

Phillips, L.F., 1981. Absolute absorption cross sections for SO between 190 and 235 nm. J. Phys. Chem. 85, 3994–4000.

Piccialli, A., Titov, D.V., Sanchez-Lavega, A., Peralta, J., Shalygina, O., Markiewicz, W.J., Svedhem, H., 2014. High latitude gravity waves at the Venus cloud tops as observed by the Venus Monitoring Camera on board Venus Express. Icarus 227, 94–111. https://doi.org/10.1016/j.icarus.2013.09.012.

Pollack, J.B., Ragent, B., Boese, R.W., Tomasko, M.G., Blamont, J., Knollenberg, R.G., Esposito, L.W., Stewart, A.I., Travis, L., 1979. Nature of the Ultraviolet Absorber in the Venus Clouds: Inferences Based on Pioneer Venus Data. Science 205 (4401), 76–79. https://doi.org/10.1126/science.205.4401.76.

Pollack, J.B., Toon, O.B., Whitten, R.C., Boese, R., Ragent, B., Tomasko, M., Eposito, L., Travis, L., Wiedman, D., 1980. Distribution and source of the UV absorption in Venus' atmosphere. J. Geophys. Res. 85, 8141–8150. https://doi.org/10.1029/JA085iA13p08141.

Ross, F.E., 1928. Photographs of Venus. ApJ 68, 57. https://doi.org/10.1086/143130.

Rossi, L., Marcq, E., Montmessin, F., Fedorova, A., Stam, D., Bertaux, J.L., Korablev, O., 2015. Preliminary study of Venus cloud layers with polarimetric data from SPICAV/VEx. Planet. Space Sci. 113114, 159–168. https://doi.org/10.1016/j.pss.2014.11.011, sI: Exploration of Venus.

Royer, E.M., Montmessin, F., Marcq, E., 2016. Variability of the nitric oxide nightglow at Venus during solar minimum. J. Geophys. Res. (Planets) 121 (5), 846–853. https://doi.org/10.1002/2016JE005013.

Sánchez-Lavega, A., Peralta, J., Gomez-Forrellad, J.M., Hueso, R., Pérez-Hoyos, S., Mendikoa, I., Rojas, J.F., Horinouchi, T., Lee, Y.J., Watanabe, S., 2016. Venus Cloud Morphology and Motions from Ground-based Images at the Time of the Akatsuki Orbit Insertion. ApJ 833 (1), L7. https://doi.org/10.3847/2041-8205/833/1/L7, 1611.04318.

Sánchez-Lavega, A., Lebonnois, S., Imamura, T., Read, P., Luz, D., 2017. The Atmospheric Dynamics of Venus. Space Sci. Rev. 212 (3–4), 1541–1616. https://doi.org/10.1007/s11214-017-0389-x.

Sander, S., Friedl, R., Barker, J., Golden, D., Kurylo, M., Wine, P., Abbatt, J., Burkholder, J., Kolb, C., Moortgat, G., et al., 2003. Chemical kinetics and photochemical data for use in atmospheric studies, evaluation number 14. JPL Publ 02 (25), 334.

Shao, W.D., Zhang, X., Bierson, C.J., Encrenaz, T., 2020. Revisiting the Sulfur-Water Chemical System in the Middle Atmosphere of Venus. J. Geophys. Res. (Planets) 125 (8), e06195. https://doi.org/10.1029/2019JE006195, 2006.09522.

Sneep, M., Ubachs, W., 2005. Direct measurement of the Rayleigh scattering cross section in various gases. J. Quant. Spectrosc. Radiat. Transfer 92, 293–310. https://doi.org/10.1016/j.jqsrt.2004.07.025.

Stiepen, A., Gérard, J.C., Dumont, M., Cox, C., Bertaux, J.L., 2013. Venus nitric oxide nightglow mapping from SPICAV nadir observations. Icarus 226 (1), 428–436. https://doi.org/10.1016/j.icarus.2013.05.031.

Titov, D.V., Svedhem, H., McCoy, D., Lebreton, J.P., Barabash, S., Bertaux, J.L., Drossart, P., Formisano, V., Haeusler, B., Korablev, O. I., Markiewicz, W., Neveance, D., Petzold, M., Piccioni, G., Zhang, T. L., Taylor, F.W., Lellouch, E., Koschny, D., Witasse, O., Warhaut, M., Acomazzo, A., Rodrigues-Cannabal, J., Fabrega, J., Schirmann, T., Clochet, A., Coradini, M., 2006. Venus Express: Scientific goals, instrumentation, and scenario of the mission. Cosm. Res. 44, 334–348. https://doi.org/10.1134/S0010952506040071.

Titov, D.V., Taylor, F.W., Svedhem, H., Ignatiev, N.I., Markiewicz, W.J., Piccioni, G., Drossart, P., 2008. Atmospheric structure and dynamics as the cause of ultraviolet markings in the clouds of Venus. Nature 456, 620–623. https://doi.org/10.1038/nature07466.

Titov, D.V., Markiewicz, W.J., Ignatiev, N.I., Song, L., Limaye, S.S., Sanchez-Lavega, A., Hesemann, J., Almeida, M., Roatsch, T., Matz, K.D., Scholten, F., Crisp, D., Esposito, L.W., Hviid, S.F., Jaumann, R., Keller, H.U., Moissl, R., 2012. Morphology of the cloud tops as observed by the Venus Express Monitoring Camera. Icarus 217 (2), 682–701. https://doi.org/10.1016/j.icarus.2011.06.020.

Toon, O.B., Pollack, J.B., Turco, R.P., 1982. The ultraviolet absorber on Venus - Amorphous sulfur. Icarus 51, 358–373. https://doi.org/10.1016/0019-1035(82)90089-6.

Vandaele, A.C., Korablev, O., Belyaev, D., Chamberlain, S., Evdokimova, D., Encrenaz, T., Esposito, L., Jessup, K.L., Lefèvre, F., Limaye, S., Mahieux, A., Marcq, E., Mills, F.P., Montmessin, F., Parkinson, C.D., Robert, S., Roman, T., Sandor, B., Stolzenbach, A., Wilson, C., Wilquet, V., 2017a. Sulfur dioxide in the Venus atmosphere: I. Vertical distribution and variability. Icarus 295, 16–33. https://doi.org/10.1016/j.icarus.2017.05.003.

Vandaele, A.C., Korablev, O., Belyaev, D., Chamberlain, S., Evdokimova, D., Encrenaz, T., Esposito, L., Jessup, K.L., Lefèvre, F., Limaye, S., Mahieux, A., Marcq, E., Mills, F.P., Montmessin, F., Parkinson, C.D., Robert, S., Roman, T., Sandor, B., Stolzenbach, A., Wilson, C., Wilquet, V., 2017b. Sulfur dioxide in the Venus Atmosphere: II. Spatial and temporal variability. Icarus 295, 1–15. https://doi.org/10.1016/j.icarus.2017.05.001.

Vlasov, P., D'Aversa, E., Belyaev, D., Ignatiev, N., Bertaux, J.L., Marcq, E., Baggio, L., Piccioni, G., Carlson, R., 2019 Ultraviolet albedo of Venus' clouds due to SPICAV and VIRTIS joint nadir observations onboard Venus Express. In: EPSC-DPS Joint Meeting 2019, vol 2019, pp EPSC-DPS2019-1597.

Watson, A.J., Donahue, T.M., Stedman, D.H., Knollenberg, R.G., Ragent, B., Blamont, J., 1979. Oxides of nitrogen and the clouds of Venus. Geophys. Res. Lett. 6 (9), 743–746. https://doi.org/10.1029/GL006i009p00743.

Yamazaki, A., Yamada, M., Lee, Y.J., Watanabe, S., Horinouchi, T., Sy, Murakami, Kouyama, T., Ogohara, K., Imamura, T., Sato, T., Yamamoto, Y., Fukuhara, T., Ando, H., Ki, Sugiyama, Takagi, S., Kashimura, H., Ohtsuki, S., Hirata, N., Hashimoto, G., Nakamura, M., 2018. Ultraviolet imager on venus orbiter akatsuki and its initial results. Earth, Planets Space 70. https://doi.org/10.1186/s40623-017-0772-6.

Zasova, L.V., Krasnopolskii, V.A., Moroz, V.I., 1981. Vertical distribution of SO_2 in upper cloud layer of Venus and Origin of U.V.-absorption. Adv. Space Res. 1 (9), 13–16. https://doi.org/10.1016/0273-1177(81)90213-1.

Zhang, X., Liang, M.C., Mills, F.P., Belyaev, D.A., Yung, Y.L., 2012. Sulfur chemistry in the middle atmosphere of Venus. Icarus 217 (2), 714–739. https://doi.org/10.1016/j.icarus.2011.06.016.